reduce the maximum (radiation-enhanced) $S_L$, which would be consistent with the observation of less increase in $S_L$ than theoretically predicted. Detailed measurements of $Y$ and $l_p$ are required to resolve this issue.

Finally, we noticed that the flame fronts appeared to be smoother when particles were added. Lean $CH_4$-air mixtures have $Le \approx 0.8$ (temperature averaged), which is low enough that they may exhibit diffusive-thermal instabilities[10] that cause flame front wrinkling when $Le$ is sufficiently low. An increase in $Le$ with increasing particle loading might be expected since the radiative transport in the optically thick regime would increase $\alpha$ but would not increase mass diffusivity. The observed trend is consistent with the notion of a higher "effective" $Le$ in particle-laden mixtures.

## Conclusions

Experiments in particle-laden gas mixtures were conducted to study flame propagation in both the optically thin and the optically thick regime of radiative transport. Data on flame shapes, propagation rates, peak pressure, maximum rate of pressure rise, and thermal decay in the burned gases were consistent with the hypothesis that at low particle loadings the particles act to increase the radiative loss from the gases, whereas at higher loadings reabsorption of emitted radiation becomes significant. This reabsorption acts to decrease the net radiative loss and augment conductive heat transport. Away from flammability limits, these effects will usually be small because the burning velocities are sufficiently high that the conductive heat flux per unit area of flame front is larger than the blackbody radiant power at the adiabatic flame temperature. In fact, very slow burning flames near flammability limits, using low-gravity conditions to suppress buoyancy effects, were required to observe these effects. Comparison with theory[7] indicated a smaller effect on burning velocity than anticipated, possibly due to the effects of the thermal capacity of the particles. Based on these results, we speculate that in sufficiently large systems, in which the absorption length is much smaller than the system size, flammability limits might not exist at $\mu g$ conditions because emitted radiation would not constitute a loss mechanism.

## Acknowledgment

This work was supported by the NASA Lewis Research Center under Grant NAG3-1242.

## References

[1]Ronney, P. D., "On the Mechanisms of Flame Propagation Limits and Extinction Processes at Microgravity," *22nd Symposium (International) on Combustion*, Combustion Institute, Pittsburgh, PA, 1988, pp. 1615–1623.

[2]Abbud-Madrid, A., and Ronney, P. D., "Effects of Radiative and Diffusive Transport Processes on Premixed Flames Near Flammability Limits," *23rd Symposium (International) on Combustion*, Combustion Institute, Pittsburgh, PA, 1990, pp. 423–431.

[3]Joulin, G., and Eudier, M., "Radiation-Dominated Propagation and Extinction of Slow, Particle-Laden Gaseous Flames," *22nd Symposium (International) on Combustion*, Combustion Inst., Pittsburgh, PA, 1989, pp. 1579–1585.

[4]Hubbard, G. L., and Tien, C. L., "Infrared Mean Absorption Coefficients of Luminous Flames and Smoke," *Journal of Heat Transfer*, Vol. 100, May 1978, pp. 235–239.

[5]Buckmaster, J. D., "The Quenching of Deflagration Waves," *Combustion and Flame*, Vol. 26, 1976, pp. 151–162.

[6]Joulin, G., and Clavin, P., "Analyse Asymptotique des conditions d'extinction des flames laminaires," *Acta Astronautica*, Vol. 3, 1976, pp. 223–240.

[7]Joulin, G., and Deshaies, B., "On Radiation-Affected Flame Propagation in Gaseous Mixtures Seeded with Inert Particles," *Combust. Sci. Tech.*, Vol. 47, 1986, pp. 299–315.

[8]Siegel, R., and Howell, J. R., *Thermal Radiation Heat Transfer*, McGraw-Hill, New York, 1972, Chap. 4.

[9]Van Vlack, L. H., *Physical Ceramics for Engineers*, Addison-Wesley, Reading, MA, 1964, Chap. 7.

[10]Williams, F. A., *Combustion Theory*, 2nd ed., Benjamin-Cummins, 1985, Chap. 9.

# Reliability Analysis of Laminated Ceramic Matrix Composites Using Shell Subelement Techniques

A. Starlinger*
*NASA Lewis Research Center, Cleveland, Ohio 44135*
D. J. Thomas†
*State University of New York, Buffalo, New York 14260*
S. F. Duffy‡
*Cleveland State University, Cleveland, Ohio 44115*
and
J. P. Gyekenyesi§
*NASA Lewis Research Center, Cleveland, Ohio 44135*

## Introduction

An updated version of the composite ceramics analysis and reliability evaluation of structures (C/CARES)[1] integrated design program was developed to use laminated shell elements in the reliability evaluation of ceramic matrix composites (CMCs). In this version of C/CARES, a subelement technique is implemented to improve the modeling of stress gradients within an element to be taken into account. The noninteractive reliability function (see Refs. 2 and 3) is now evaluated at each Gaussian integration point instead of using averaging techniques. As a result of the increased number of stress evaluation points, considerable improvements in the accuracy of reliability analyses have been realized.

Because of the relatively small thickness in comparison to the overall dimensions of typical laminated CMC material systems, components fabricated from this material are conveniently modeled using shell elements. In the formulation of standard shell elements, classical lamination theory is usually adopted to describe the mechanical behavior. Finite element algorithms exactly determine the stresses at the Gaussian integration points of a shell element where the local stiffness matrix is evaluated. For this reason the concept of subelements is introduced in the new version of C/CARES, whereby the risk of rupture intensity is evaluated at each Gaussian integration point instead of using averaging techniques. This method defines a corresponding subelement for each Gaussian integration point. The subelement volume is defined as the contribution of the integration point to the element volume and is determined by the numerical integration procedure associated with the shell element. Thus, each ply in the laminate is divided into subelements, and the risk of rupture intensity function $\psi$ is evaluated for the corresponding stress tensor at each integration point. The number of subelements in each element depends on the element type and on the order of integration chosen. By using the subelement technique, as opposed to averaging the stresses across the element, stress variations within a component can be better modeled. As a

Presented as Paper 92-2348 at the AIAA/ASME/ASCE/AHS/ASC Structures, Structural Dynamics, and Materials Conference, Dallas, TX, April 13–15, 1992; received Sept. 12, 1992; revision received March 19, 1993; accepted for publication March 20, 1993. 

*Research Associate, National Research Council.
†Department of Mechanical and Aerospace Engineering, Ohio Aerospace Institute.
‡Department of Civil Engineering.
§Department of Engineering, NASA Lewis Resident Research Associate.

result, components with high stress gradients, or with distorted mesh geometries, can be analyzed with coarser meshes than otherwise necessary (provided that the mesh density is sufficient to give accurate stresses at the integration points).

The C/CARES algorithm requires prior knowledge of the stress field throughout a component; and, therefore, it is designed as a postprocessor to be run in conjunction with commercially available finite element packages that determine the structural response of the component to thermomechanical loads. For versatility, the C/CARES code is divided into two modules. The first module interfaces with the finite element results and translates the output into a formatted (ASCII) neutral data base for use in the subsequent reliability analysis. The second module performs the computations necessary in determining the component reliability. Because of the subelement concept, a global structure has evolved for the C/CARES algorithm. The introduction of a single large, blank common array (instead of several fixed-dimension arrays) in the reliability module allows the user to easily adapt the program to the mesh size necessary for a given component and to the available computational resources. Since the program has been developed in a modular structure, future changes and additions (such as the introduction of more sophisticated reliability models) will not involve large programming efforts.

## Neutral Data Base Concept

The formatted neutral data base allows C/CARES to be interfaced with several finite element programs. At the present time, interface programs for MARC and MSC/NASTRAN have been implemented. Interfaces for ABAQUS and ANSYS are being prepared. The structure of the neutral data base is optimized with respect to memory. The finite element data are arranged within the neutral data base by using the following hierarchy: element groups, elements, and subelements. Element groups may be user defined such that each group is comprised of elements of a given element type, laminate structure, etc. Additionally, if the reliability analysis is focused on a specific region of a component (e.g., a region containing a stress concentration), the corresponding elements can be combined into an element group. This segment of the data base contains information regarding which elements are associated with each group, as well as the total number of elements within each group. Information pertaining to the elements includes the number of subelements (integration points) and the number of plies associated with each element. Finally, the subelement data contain information regarding ply identification, ply subvolume, ply stress state (assuming plane stress conditions), ply temperature, and ply material type. Note that a subelement can have more than one ply.

Typically, ply volumes are not included with standard finite element output. Thus, the volume of each subelement (corresponding to a Gaussian integration point) is calculated by using the shape functions inherent to the element type to determine the midsurface area and then multiplying by the layer thickness. Currently, bilinear (four nodes) and biquadratic (eight nodes) element shape functions are used to determine the subelement areas.

The midsurface area of a shell element is calculated by integration in natural space (see Bathe[4] for details)

$$A = \int_{-1}^{1} \int_{-1}^{1} \det J(r,s)\,dr\,ds \tag{1}$$

where $J$ is the Jacobian operator and $r$ and $s$ are natural coordinates. By applying a Gaussian integration scheme, this integral can be expressed as

$$A = \sum_{i=1}^{m} \sum_{j=1}^{m} \det J(r_i,s_j) W_i W_j \tag{2}$$

where $m$ is the integration order, $r_i$ and $s_j$ are the coordinates of the Gaussian integration points in natural space, and the $W$ are weight functions. The Jacobian operator $J$ is calculated by using the corresponding element shape functions, element connectivities, and global coordinates of the element nodes. The area of the subelement corresponding to the integration point $i,j$ represents one term in the summation [Eq. (2)].

## Reliability Modeling

The reliability analysis requires knowledge of the stress state of each ply subelement, the ply subvolume, the local temperature, and the temperature-dependent Weibull parameters. Based on this information, the subelement reliability is expressed as

$$R_i^{\text{sub}} = \exp(-\psi_i^{\text{sub}} V_i^{\text{sub}}) \tag{3}$$

where $\psi_i^{\text{sub}}$ is the value of the risk of rupture intensity within the subelement of the $i$th ply. Similarly, $V_i^{\text{sub}}$ is the volume of the subelement of the $i$th ply.

The value of the risk of rupture intensity $\psi_i^{\text{sub}}$ is determined using Eq. (4).[3] The Weibull parameters $\alpha^T(t)$, $\alpha^C(t)$, $\beta^T(t)$, $\beta^C(t)$, and $\gamma(t)$ are calculated with respect to the local temperature $t$ by linear interpolation of the material parameters specified in a control file. The superscripts $T$ and $C$ represent tensile and compressive properties, respectively.

$$\psi_i^{\text{sub}}(x,y,z,t) = \left[ \left( \frac{\langle \sigma_1 - \gamma_1^T \rangle}{\beta_1^T} \right)^{\alpha_1^T} + \left( \frac{\langle -\sigma_1 + \gamma_1^C \rangle}{\beta_1^C} \right)^{\alpha_1^C} + \left( \frac{\langle \sigma_2 - \gamma_2^T \rangle}{\beta_2^T} \right)^{\alpha_2^T} + \left( \frac{\langle -\sigma_2 + \gamma_2^C \rangle}{\beta_2^C} \right)^{\alpha_2^C} + \left( \frac{\langle |\sigma_{12}| - \gamma_{12} \rangle}{\beta_{12}} \right)^{\alpha_{12}} \right]_i \tag{4}$$

We define the following notation used in Eq. (4):

$$\langle x \rangle \equiv x \cdot u[x] = \begin{cases} 0, & x \le 0 \\ x, & x > 0 \end{cases} \tag{5}$$

where $u[x]$ is the unit step function.

Survival of the subelements are assumed to be independent processes; thus, using a weakest link theory (WLT), the reliability of each ply $i$ is given as the product of all subelement reliabilities within the model

$$R_i = \prod_k (R_i^k) = \exp\left[ -\sum_k (\psi_i^{\text{sub}})_k (V_i^{\text{sub}})_k \right] \tag{6}$$

where $k$ is the total number of all subelements. Similarly, the overall component reliability ($R^{\text{WLT}}$) can be expressed as the product of the individual ply reliabilities. Alternatively, Thomas and Wetherhold[3] proposed an upper bound limit to the reliability estimate using a strongest link theory (SLT). Expressions for both approaches are given below for an $n$ ply laminate.

$$R^{\text{WLT}} = \prod_{i=1}^{n} R_i \qquad R^{\text{SLT}} = 1 - \prod_{i=1}^{n} (1 - R_i) \tag{7}$$

After the reliability analysis is performed, the data for the risk of rupture intensity (a local measure of the probability of failure) can be stored in a PATRAN element file. This allows graphical representation, in the form of contour plots, of critical design regions in the structure. Note that PATRAN can only assimilate element (and not subelement) information. Thus, the element risk of rupture intensity is approximated by averaging all subelements within the element using the following expression:

$$\psi_i^{\text{ele}} = \frac{\sum_{k=1}^{n\text{sub}} \psi_i^k V_i^k}{\sum_{k=1}^{n\text{sub}} V_i^k} \tag{8}$$

where $n$sub is the number of subelements within the element. The values for $\psi_i^{\text{ele}}$ are only used for PATRAN postprocessing.

## Numerical Examples

To illustrate the improvements achieved by the updated version of C/CARES, the problem of a plate with a hole was analyzed. This example had previously been studied in-house at NASA Lewis Research Center using MSC/NASTRAN. By interfacing C/CARES with the MARC finite element program, which provides the user with stress output at the integration points, we were able to implement the new subelement capabilities and compare the reliability analyses based on these results with those obtained using stresses averaged over the element (i.e., MSC/NASTRAN results where only centroidal information is available to the user). Specifically, a laminated CMC plate with a central circular hole was subjected to prescribed edge displacements at room temperature (see Fig. 1). The elastic material properties are presented in Table 1. The laminate consisted of eight unidirectional orthotropic plies with a $[0/\pm 45/90]_s$ ply layup. Note that, because experimental strength data was lacking, heuristic values for $\alpha^T(t)$, $\alpha^C(t)$, $\beta^T(t)$, $\beta^C(t)$, $\gamma^T(t)$, and $\gamma^C(t)$ were used (see Table 2). To model this quasi-two-dimensional problem, appropriate degrees of freedom were restrained in each analysis. Two mesh densities were used for the finite element analysis of this problem. The coarse mesh contained 1000 elements, and a more dense mesh contained 2520 elements. Thus, in all, four example cases were run (MARC: 1000 and 2520 elements; MSC/NASTRAN: 1000 and 2520 elements). A $2\times 2$ integration scheme was used for both MARC analyses (four subelements for each shell element).

In Table 3, the component reliabilities $R^{WLT}$ are given for all four analyses. The component reliability results based on SLT were nearly unity for all four cases and, therefore, were not included in the table. In Table 4 the reliability results for each ply $R_i$ based on the MARC analysis (dense mesh) are compared to the ply reliabilities as determined using the MSC/NASTRAN analysis (dense mesh).

**Table 1 Elastic Properties**

| | |
|---|---|
| Young's modulus in fiber direction $E_1$, MPa | 19,755.0 |
| Young's modulus transverse to fiber direction $E_2$, MPa | 1975.5 |
| Shear modulus $G_{12}$, $G_{13}$, $G_{23}$, MPa | 700.0 |
| Poisson ratio $\nu_{12}$ | 0.35 |

**Table 2 Weibull Strength Parameters**

| Failure mode | $\alpha$ | $\beta$, MPa | $\gamma$, MPa |
|---|---|---|---|
| Fiber direction: | | | |
| Tensile, $\sigma_f^{T,\max}$ | 25 | 450 | 0 |
| Compressive, $\sigma_f^{C,\max}$ | 35 | 4500 | 0 |
| Transverse direction: | | | |
| Tensile, $\sigma_t^{T,\max}$ | 10 | 350 | 0 |
| Compressive, $\sigma_t^{C,\max}$ | 30 | 3500 | 0 |
| Inplane shear, $\sigma_{ft}^{\max}$ | 22 | 420 | 0 |

**Table 3 Comparison of different reliability analyses**

| Number of elements | Component reliability, $R^{WLT}$ | |
|---|---|---|
| | MARC | MSC/NASTRAN |
| 1000 | 0.9005 | 0.9304 |
| 2520 | 0.8991 | 0.9276 |

**Table 4 Ply by ply reliabilities**

| Ply orientation $\theta$, deg | Ply reliabilities | |
|---|---|---|
| | MSC/NASTRAN, (2520 elements) | MARC, 2520 elements |
| 0 | 0.96587 | 0.94652 |
| +45 | 0.99999 | 0.99999 |
| −45 | | |
| 90 | | |
| 90 | | |
| −45 | | |
| +45 | ▼ | ▼ |
| 0 | 0.96587 | 0.94652 |

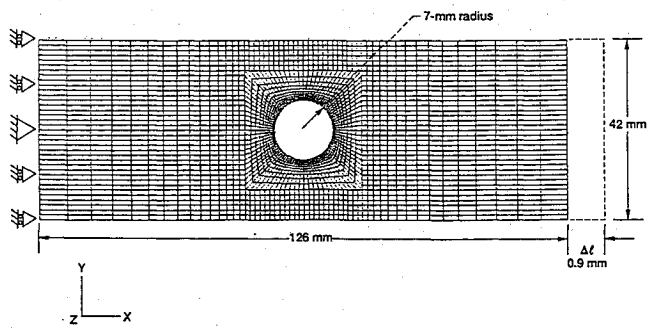


**Fig. 1 Finite element mesh for $[0/\pm 45/90]_s$ laminate, ply thickness $h$, 0.2 mm.**

The reliability analyses using MARC results yielded smaller component reliabilities for both the coarse and the dense meshes relative to the respective MSC/NASTRAN analyses. The decrease in predicted component reliability is a consequence of the more accurate reliability computations in the region of the stress concentration which were made possible by using the stresses at the integration points. In the high stress regions, where the stress gradients are also very large, the stress solution may be underestimated by a greater degree in the MSC/NASTRAN analysis due to stress averaging over a larger region (i.e., averaging over the whole element as opposed to the smaller subelement). This results in incorrectly predicting a higher component reliability for this problem. The MARC results show that the mesh density is sufficiently fine, even for the coarse mesh, to determine stresses accurately at the integration points. The agreement between the four cases in the prediction for $R^{SLT}$ is due to the high reliabilities of plies 2–7 dominating the calculation of $R^{SLT}$ [see Eq. (7)].

## Conclusion

Based on the previous version of C/CARES, an enhanced version of this integrated design program was developed for the reliability evaluation of ceramic matrix composite (CMC) laminated shell components. By dividing the original program into two separate modules, more flexibility was achieved, allowing for easy implementation with various finite element programs. As a result of the introduction of a shell subelement technique, the number of reliability function evaluation points per element was increased. A numerical example demonstrated improvements in the accuracy of reliability analyses. The new version allows structural components to be modeled with coarser finite element meshes than those required by the previous version of the program and still achieve the same order of accuracy. The modular structure of the program allows the design engineer to incorporate additional reliability functions without major programming efforts. Future versions of C/CARES will focus on this issue.

## References

[1]Duffy, S. F., Palko, J. L., and Gyekenyesi, J. P., "Structural Reliability Analysis of Laminated CMC Components," *Journal of Engineering for Gas Turbines and Power,* Vol. 115, No. 1, 1993, pp. 103–108.

[2]Duffy, S. F., and Manderscheid, J. M., "Noninteractive Macroscopic Reliability Model for Ceramic Matrix Composites with Orthotropic Material Symmetry," *Journal of Engineering for Gas Turbines and Power,* Vol. 112, No. 4, 1990, pp. 507–511.

[3]Thomas, D. J., and Wetherhold, R. C., "Reliability Analysis of Continuous Fiber Composite Laminates," *Composite Structures,* Vol. 17, No. 4, 1991, pp. 277–293.

[4]Bathe, K. J., *Finite Element Procedures in Engineering Analysis,* Prentice-Hall, Englewood Cliffs, NJ, 1982, p. 204.